

High-power pulse trains excited by modulated continuous waves

Yan Wang¹, Lijun Song², Lu Li^{1*} and Boris A. Malomed³

¹*Institute of Theoretical Physics, Shanxi University, Taiyuan 030006, China*

²*College of Physics and Electronics Engineering, Shanxi University, Taiyuan 030006, China and*

³*Department of Physical Electronics, School of Electrical Engineering, Faculty of Engineering, Tel Aviv University, Tel Aviv 69978, Israel*

Pulse trains growing from modulated continuous waves (CWs) are considered, using solutions of the Hirota equation for solitons on a finite background. The results demonstrate that pulses extracted from the maximally compressed trains can propagate preserving their shape and forming robust arrays. The dynamics of double high-power pulse trains produced by modulated CWs in a model of optical fibers, including the Raman effect and other higher-order terms, is considered in detail too. It is demonstrated that the double trains propagate in a robust form, with frequencies shifted by the Raman effect.

I. INTRODUCTION

Recently, solitons on a finite background, generated by the fundamental nonlinear Schrödinger (NLS) equation with self-focusing, which have been known for a long time, have drawn renewed interest as prototypes of rogue waves in the ocean [1–6], optical fibers [7–12], plasmas [13] and other nonlinear media. NLS solutions for solitons on a finite background can be identified as the Kuznetsov-Ma soliton (KMS) [14, 15], which is localized in the transverse direction, the Akhmediev breather (AB) [16], localized in the longitudinal direction, and the Peregrine solution (PS) [17], which is a limit case of the KMS and AB, being localized in both the transverse and longitudinal directions. The spatiotemporal localization predicted by the PS solution, and dynamical manifestations of the KMS have been demonstrated in optical fibers [9, 10]. Splitting of the PS produced by deformed initial conditions, and the related modulational instability have been observed too [11, 12]. The dynamics accounted for by the AB was first observed in Ref. [18] and further analyzed in Ref. [9]. Collisions between ABs [19], their dynamics in optical fibers with a longitudinally tailored dispersion [20], and shaping of an optical frequency comb into a generator of rogue waves [21] have been demonstrated too. In these experiments, the ABs and KMSs were excited by weakly and strongly modulated continuous waves (CWs), respectively.

Generally, NLS solutions initiated by perturbations added to a finite background feature strong temporal compression of emerging peaks [22]. In optical systems, such dynamical scenarios can be used for the generation of supercontinuum, and of high-power ultrashort pulses and pulse trains [18, 23–26].

To create high-repetition-rate and high-quality pulse trains, the delay-line interferometer was used to eliminate the finite background around the AB and allow doubling of the repetition rate of the pulse trains [27].

A possibility of spontaneous transformation of ABs into solitons and ultrashort pulses generated by the modulation instability have been considered too [28, 29]. Extraction of high-power optical pulses from the PS by means of the spectral-filtering method was proposed in Refs. [30–32]. However, these results are only suitable for picosecond pulses with the width $\gtrsim 5$ ps [33, 34]. In the present paper, using soliton solutions on the finite background for the Hirota equation, we construct high-power strongly compressed pulse trains induced by modulated CWs in the subpicosecond regime, an appropriate model for which must include higher-order terms, added to the usual NLS equation.

The paper is organized as follows. In Sec. II, the Hirota equation, which models the pulse propagation in the nonlinear fiber, is presented, and solutions for solitons on the finite background are recapitulated for this equation. In the same section, using AB and KMS solutions for the Hirota equation, high-power compressed pulse trains induced by modulated CWs are demonstrated in the model with the higher-order terms, making use of juxtaposition of two solutions with a half-period temporal shift and opposite signs. The influence of the Raman effect on the high-power pulse trains is considered in Sec. III. Conclusions are summarized in Sec. IV.

II. HIGH-POWER PULSE TRAINS PRODUCED BY THE HIROTA EQUATION

As said above, the standard NLS equation is valid as the model for picosecond pulses with the width $\gtrsim 5$ ps, while in the subpicosecond or femtosecond regime higher-order terms should be included, to account for the third-order dispersion (TOD), self-steepening, and the Raman effect [33, 34]. This accordingly modified NLS equation is

$$\frac{\partial A}{\partial z} + i \frac{\beta_2}{2} \frac{\partial^2 A}{\partial T^2} - \frac{\beta_3}{6} \frac{\partial^3 A}{\partial T^3} = i\gamma \left[|A|^2 A + \frac{i}{\omega_0} \frac{\partial |A|^2 A}{\partial T} - (i\alpha_\nu + T_R) A \frac{\partial |A|^2}{\partial T} \right]. \quad (1)$$

*Electronic address: llz@sxu.edu.cn

Here $A = A(z, T)$ is the slowly varying envelope of the electric field, $T = t - z/v_g \equiv t - \beta_1 z$, where t and z are the temporal variable and propagation distance, and v_g is the group velocity. Coefficients β_2 , β_3 , γ , α_ν and T_R account for the second-order group-velocity dispersion (GVD), TOD, strength of the Kerr nonlinearity, nonlinear dispersion, and the Raman time-delay constant, respectively. Equation (1) does not include the fiber loss, assuming, as usual, that it may be compensated by gain [33, 34]. At the end of Sec. III, we produce results of the analysis of the model which explicitly includes the loss, the conclusion being that the difference is relatively small except for a decreasing of peak power.

By means of rescaling, $A(z, T) \equiv \sqrt{P_0}q(\xi, \tau)$, $\tau \equiv T/T_0$, and $\xi = z/L_D$, with the temporal scale $T_0 = [|\beta_2|/(\gamma P_0)]^{1/2}$ and dispersion length $L_D = (\gamma P_0)^{-1}$, Eq. (1) is transformed into

$$\begin{aligned} \frac{\partial q}{\partial \xi} = & i \left(\frac{s}{2} \frac{\partial^2 q}{\partial \tau^2} + |q|^2 q \right) + \alpha_3 \frac{\partial^3 q}{\partial \tau^3} \\ & + \alpha_4 \frac{\partial |q|^2 q}{\partial \tau} + (\alpha_5 - i\tau_R) q \frac{\partial |q|^2}{\partial \tau}, \end{aligned} \quad (2)$$

where $s \equiv -\beta_2/|\beta_2|$ is +1 and -1 for the anomalous and normal GVD, respectively, and the other coefficients are

$$\alpha_3 = \frac{\beta_3}{6|\beta_2|T_0}, \alpha_4 = -\frac{1}{\omega_0 T_0}, \alpha_5 = \frac{\alpha_\nu}{T_0}, \tau_R = \frac{T_R}{T_0}, \quad (3)$$

which, as well as their unscaled counterparts, are related to the TOD, self-steepening, nonlinear dispersion, and the Raman effect, respectively. In its general form, Eq. (2) is not integrable. However, if the Raman effect is omitted, i.e., $\tau_R = 0$, and additional conditions

$$\alpha_4 = 6\alpha_3, \quad \alpha_4 + \alpha_5 = 0, \quad (4)$$

are satisfied, Eq. (2) becomes the integrable Hirota equation [35]. Here we only consider the case of the anomalous GVD, i.e. $s = 1$. In this case, the solution of the Hirota equation for a soliton placed on top of a finite background can be compactly written as [22, 36, 37]

$$q(\xi, \tau) = \left[1 + \frac{2(1-2a) \cosh(b\xi) + ib \sinh(b\xi)}{\sqrt{2a} \cos[\omega(\tau + c\xi)] - \cosh(b\xi)} \right] e^{i\xi}, \quad (5)$$

$$\omega = 2\sqrt{1-2a}, \quad b = \sqrt{8a(1-2a)}, \quad c = 2(1+4a)\alpha_3, \quad (6)$$

where a is a real constant parametrizing this class of the solutions [10]. When $\alpha_3 = 0$, solution (5) goes over into its NLS counterpart [10].

For $0 < a < 1/2$, constants ω , b and c in Eq. (5) are real. In this case, the solution describes the AB, and the maximally compressed pulse train is attained at point $\xi = 0$, in the form of

$$q_{\max}(\tau) = \frac{1 - 4a + \sqrt{2a} \cos(\omega\tau)}{\sqrt{2a} \cos(\omega\tau) - 1}, \quad (7)$$

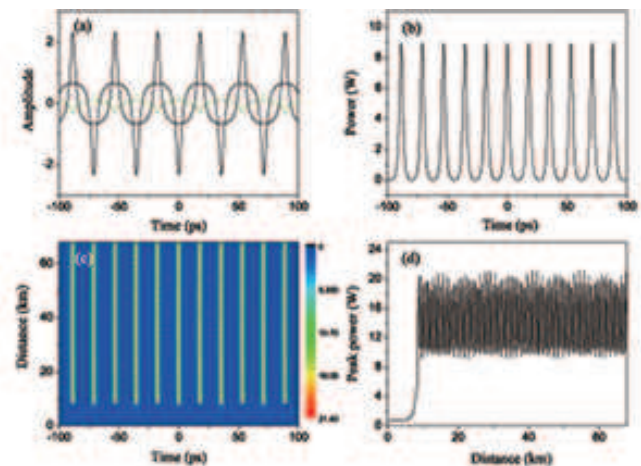


FIG. 1: (Color online) (a) The maximally compressed pulse train at $z = 8.4206$ km, juxtaposed with its counterpart with the opposite sign, delayed by a half a period. Here the blue dotted and green dashed-dotted curves depict, respectively, the real and imaginary parts of the numerical result, while the black solid curve shows the exact solution, which actually overlaps with the blue dotted curve. (b) The intensity distribution of the resulting double pulse train, produced as the superposition of the two original trains. (c) The evolution of the double train with zero background. (d) The evolution of the peak power of the double train with zero background. These results correspond to $a = 0.4$ in Eq. (6) and $\delta = 0.01$ in Eq. (9).

with period $2\pi/\omega$ and background power

$$P_{\text{bg}} = (2\sqrt{2a} - 1)^2, \quad (8)$$

which corresponds to $\cos(\omega\tau) = -1$. The analysis reported in Ref. [20] has demonstrated that, in the range of $0 < a < 0.2$, the evolution of the maximally compressed pulse train can be frozen with the help of a specifically tailoring the GVD profile, which leads to formation of a quasi-stable train of fundamental solitons, while at $a > 0.2$ a delay-line interferometer can be used to create a high-power pulse train with the double repetition rate and zero background, as shown in Ref. [27].

A natural question is whether such a double-repetition-rate high-power train can stably propagate in the framework of the fiber model. To address this issue, it is necessary to choose suitable initial conditions, which can excite a maximally compressed pulse array similar to the AB profile (7). It has been shown that such a maximally compressed pulse train can be excited by a modulated CW [11, 38], corresponding to the initial condition

$$q(0, \tau) = \sqrt{1 + \delta \cos(\omega\tau)}, \quad (9)$$

where δ is a small modulation amplitude, and ω is the modulation frequency, taken as per Eq. (6).

We numerically simulated the integrable Hirota equation with the initial modulated CW state (9), where the system parameters are adjusted to the SMF-28 fiber with

$\beta_2 = -21.4 \text{ ps}^2\text{km}^{-1}$, $\beta_3 = 0.12 \text{ ps}^3\text{km}^{-1}$, and $\gamma = 1.2 \text{ W}^{-1}\text{km}^{-1}$ around 1550 nm [11], and the initial power $P_0 = 0.7 \text{ W}$. The simulations are necessary, as generic solutions of equations cannot be obtained in an explicit analytical form. In fact, high-power pulse trains growing from the modulated CW do not necessarily reduce to exact breather solutions of the Hirota equation, such as KMS [27]. In the present case, the normalized parameters are $T_0 = 5.0474 \text{ ps}$, $L_D = 1.1905 \text{ km}$, and $\alpha_3 = 1.8516 \times 10^{-4}$, respectively. The simulation demonstrates that the maximally compressed pulse train is attained at $z = 8.4206 \text{ km}$, as shown in Fig. 1(a). At this position, we superpose the train and its counterpart with the opposite sign, delayed by half a period, to produce a double pulse train, which is displayed in Fig. 1(b). The procedure can be experimentally realized by using a delay line and a piezo-electrical device to impose the necessary delay of the pulse train and the π phase-shift, as shown in Ref. [27]. Then, we let the resulting pulse train propagate in the fiber, see the corresponding stable regime in Fig. 1(c). Unlike its exact counterpart, the numerical solution at the point of the strongest compression includes an imaginary part [shown by the green dashed-dotted curves in Fig. 1(a)], whose maximum value is $0.0985 \approx 1\%$ of the amplitude in the real part, which is a small perturbation that was included to test the stability of the propagation of the pulse train with the zero background. Because the soliton number, $N \equiv [\gamma P(\Delta\tau/1.763)^2/|\beta_2|]^{1/2}$, takes value 1.3617 for the present parameter set, which exceeds 1, individual pulses in the resulting train, with peak power P and full-width at half-maximum (FWHM) $\Delta\tau = 3.3878\text{ps}$, exhibit oscillations, as shown in Fig. 1(d). We stress that the oscillatory regime is a dynamically stable one, as is clearly shown by the simulations.

Next, we turn to the case of $a > 1/2$, which corresponds to the high background power, as per Eq. (8). In this case, Eq. (6) yields imaginary ω and b , converting the hyperbolic and trigonometric functions in Eq. (5) into trigonometric and hyperbolic ones, respectively, thus swapping localization and periodicity features of the solution. It now represents a bright oscillating pulse propagating on top of a finite background, which is generally classified as KMS. Accordingly, the maximally compressed pulse is attained at $\xi = 0$

$$q_{\max}(\tau) = \frac{1 - 4a + \sqrt{2a} \cosh(\tilde{\omega}\tau)}{\sqrt{2a} \cosh(\tilde{\omega}\tau) - 1}, \quad (10)$$

with $\tilde{\omega} = 2(2a - 1)^{1/2}$. This pulse has a single peak at $\tau = 0$ [$q_{\max}(0) = -(1 + 2\sqrt{2a})$], and background value $q = 1$ as $|\tau| \rightarrow \infty$, which makes the solution completely different from the AB.

In principle, the maximally compressed pulse can be created by a small localized sech-type perturbation added to a CW background [22]. On the other hand, it was demonstrated in Ref. [10] that such a pulse can be ex-

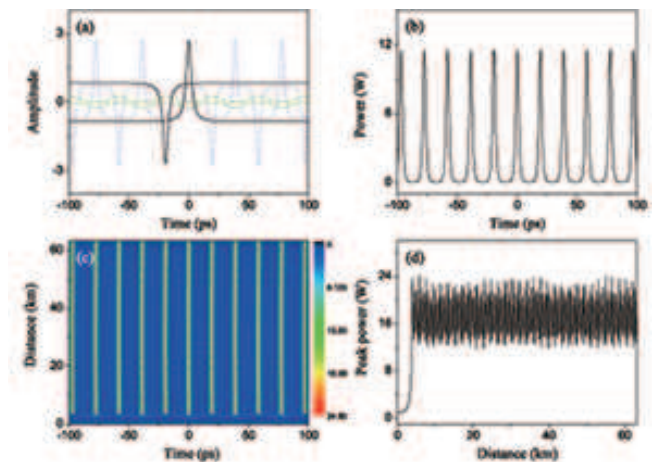


FIG. 2: (Color online) (a) The maximally compressed pulse train at $z = 3.7080 \text{ km}$ and its counterpart with the opposite sign and temporal delay π/Ω . (b) The intensity distribution of the train produced by the juxtaposition of both original trains. (c) The evolution of the resulting pulse train with zero background. (d) The evolution of the peak power of the resulting pulse train with zero background. Here $a = 0.6$. The notation adopted in the panels is the same as in Fig. 1.

cited by a strongly modulated CW in the form of

$$q(0, \tau) = 1 + A [1 + \cos(\Omega\tau)] \quad (11)$$

with $\Omega = \tilde{\omega} \cos^{-1}[(\sqrt{4a - 2\sqrt{2a} + 1} - 1)/(\sqrt{2a} - 1) - 1]/\cosh^{-1}\{1[(4a - 2)/(\sqrt{4a - 2\sqrt{2a} + 1} - 1) - 1]/\sqrt{2a}\}$ and $A = \sqrt{2a} - 1$, which has the peak power and FWHM identical to those of the intensity profile, $|q_{\min}(\tau)|^2 = \{1 + [2(2a - 1)]/[\sqrt{2a} \cosh(\tilde{\omega}(\tau + c\pi/\tilde{b})) + 1]\}^2$, at the point of the minimal intensity, $\xi = \pi/b$, where $b = [8a(2a - 1)]^{1/2}$.

Starting from input (11), we have simulated, similar to what is shown above in Fig. 1, the evolution produced by the juxtaposition of the maximally compressed pulse trains and its counterpart with the opposite sign and half-a-period delay. The results, summarized in Fig. 2, show that, for our choice of the parameters, the maximally compressed pulse train is attained at $z = 3.7080 \text{ km}$ [Fig. 2(a)], with individual pulses in the train being almost identical to the profile of the maximally compressed pulse given by Eq. (10). Thus, combining the pulse train with its counterpart with the opposite sign and time delay π/Ω , one can construct a double pulse train with zero background [see Fig. 2(b)]. It propagates stably, exhibiting oscillatory behavior of the pulses, as the respective soliton number is $N = 1.2761$, with FWHM $\Delta\tau = 2.7927 \text{ ps}$, which again exceeds 1, see Figs. 2(c) and (d). Similarly, unlike the exact solution, the numerical result includes an imaginary part [see the green dash dotted curves in Fig. 2(a)], with maximum value $0.0583 \approx 0.76\%$ of the amplitude of the real part, which does not affect the stable propagation of the pulse train with zero background.

Finally, it should be pointed out that, in the case of $a \rightarrow 1/2$, solution (5) of the Hirota equation reduces to the PS in the form of

$$q(\xi, \tau) = \left[1 - \frac{4(1 + 2i\xi)}{1 + 4\xi^2 + 4(\tau + 6\alpha_3\xi)^2} \right] e^{i\xi},$$

which is a superposition of the CW solution and a rational fraction function, forming a maximally compressed pulse at $\xi = 0$ [17, 30]. This implies that the Peregrine rogue wave, i.e., the maximally compressed pulse, can be excited by a small localized (single-peak) perturbation placed on top of the CW background [22]. Thus, the high-power pulse extracted from the Peregrine rogue wave can be realized by means of the spectral-filtering method, displaying a breather-like behavior [31, 32].

III. THE INFLUENCE OF THE RAMAN EFFECT ON HIGH-POWER PULSE TRAINS

In the previous Section, we have considered the generation and propagation of the pulse trains growing from the CWs as solutions of the Hirota equation, i.e., Eq. (2) under the integrability relations (4), while the Raman effect was not included ($\tau_R = 0$). This model does not precisely apply to real optical fibers, but the exact solutions provided by it help one to understand the pulse-train dynamics in more general models.

In this section, we report results of simulations of Eq. (2) with realistic values of parameters (3), including a nonzero Raman coefficient, and without imposing integrability conditions (4): $\alpha_3 = 1.8516 \times 10^{-4}$, $\alpha_4 = -1.6292 \times 10^{-4}$, α_5 is determined by the delayed-nonlinear-response parameter α_ν , and $\tau_R = 5.9437 \times 10^{-4}$ for the usual value of the Raman time constant, $T_R = 3$ fs. Actually, α_ν is a small quantity which has little effect on simulation results, therefore we set $\alpha_\nu = 0$. Thus, we focus on the influence of the Raman effect on the dynamics of the high-power pulse trains growing from the modulated CWs introduced as per Eqs. (9) and (11).

In the analysis presented above the modulation amplitude A and frequencies ω and Ω in Eqs. (9) and (11) were taken as functions of parameter a , making it possible to compare the results with the exact solutions produced by the Hirota equation, as shown in Fig. 1(a) and Fig. 2(a). However, in the realistic fiber-optic model, the modulation amplitudes and frequencies can take arbitrary values. Here, we use inputs given by Eqs. (9) and (11) with different values of the parameters, aiming to excite the maximally compressed pulse trains, and perform subsequent simulations of the corresponding double pulse trains in the framework of Eq. (2).

Fig. 3 shows the evolution of the train initiated by input (9) with $\delta = 0.03$ and $\omega = 1$. In Fig. 3(a) one can see that the modulated CW initially undergoes strong temporal compression and increase of the peak power, attaining the maximally compressed state of the train at $z = 6.5277$ km. At that stage, the double

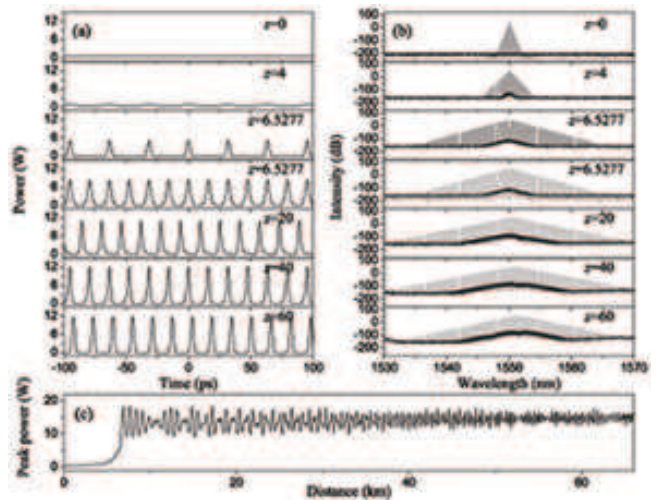


FIG. 3: (Color online) (a) Power profiles at different propagation distances for the pulse train generated by the modulated CW given by Eq. (9). (b) The corresponding power spectra. (c) The evolution of the peak power. Here the parameters are $\delta = 0.03$, $\omega = 1$, $T_R = 3$ fs, and $\alpha_\nu = 0$.

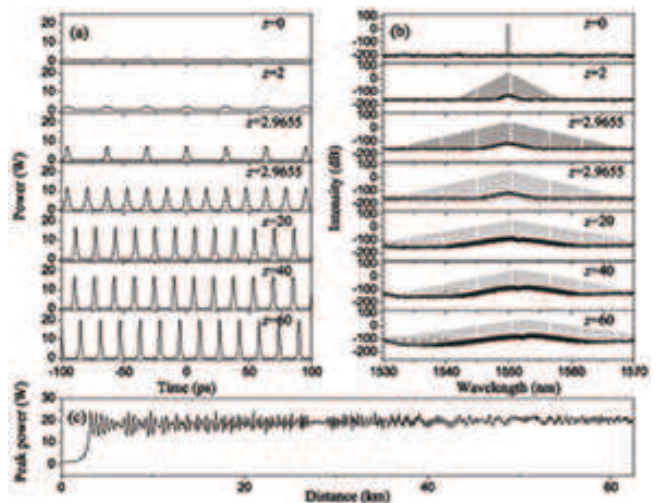


FIG. 4: (Color online) The same as in Fig. 3, but for the pulse train generated by the input in the form of Eq. (11). The parameters are $A = 0.13$, $\Omega = 1$, $T_R = 3$ fs, and $\alpha_\nu = 0$.

pulse train is constructed, using the delay-line interferometer (the method is outlined in the previous Section, see also Ref. [27]), which robustly propagates along the fiber. Fig. 3(b) displays the concomitant evolution of the pulse-train's power spectrum, showing that the spectrum initially expands until the point of the maximum compression, at which the spectral distribution is reduced to a half of the original spectrum [27]. Subsequently, the spectral width remains essentially constant, while the frequencies feature the red shift induced, as usual, by the Raman effect [33, 34]. For the presently chosen parameters, the frequency shift of the train is about 1.1967 THz at 60 km. In addition, the evolution of the peak power,

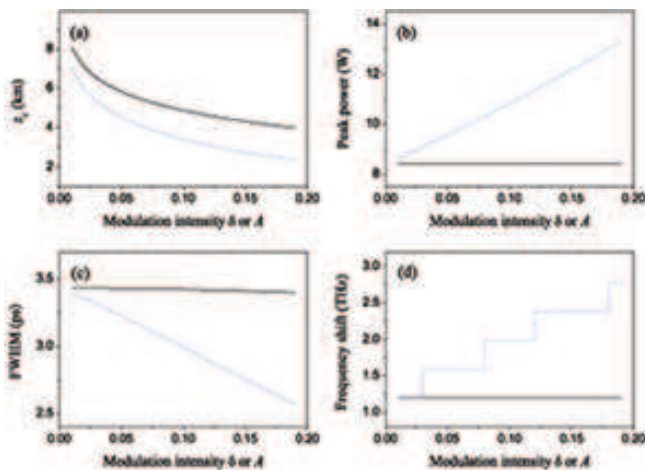


FIG. 5: (Color online) (a) The position of the maximally compressed pulse train, (b) the peak power, (c) the FWHM of the central pulse in the double pulse train, and (d) the Raman-induced frequency shift after passing 60 km in the fiber, versus the modulation intensity δ or A , with the black solid and blue dotted curves pertaining to inputs (9) and (11), respectively. Here the parameters are $\Omega = \omega = 1$, $T_R = 3$ fs, and $\alpha_\nu = 0$.

which exhibits an oscillatory behavior, is displayed in Fig. 3(c).

Fig. 4 displays the evolution initiated by the input given by Eq. (11) with $A = 0.13$ and $\Omega = 1$. This scenario exhibits three differences in comparison with Fig. 3. One is that the maximally compressed pulse train is attained at a shorter distance, i.e., $z = 2.9655$ km, as seen in Fig. 4(a). The other is that the initial spectrum is narrower, while the Raman-induced red frequency shift is larger, as seen in Fig. 4(b), in which the frequency shift of the train is about 2.3854 THz at 60 km. The third difference is a higher peak power, as seen in Fig. 4(c).

To summarize the dynamical results outlined above, in Fig. 5 we present the largest-compression position z_c for the pulse trains, their peak power, the FWHM of the central pulse in the double pulse trains constructed with the help of the delay-line interferometer method, and the corresponding frequency shift accumulated after the 60 km long propagation, as functions of parameters δ and A in inputs (9) and (11), respectively.

In Fig. 5(a), one can see that, for the same modulation intensity, the position of the strongest compression corresponding to initial condition (11) is always smaller than its counterpart corresponding to input (9). Interestingly, for the double pulse train induced by the latter input, the peak power and the FWHM of the central pulse are almost constant for the present parameters, which leads to the nearly constant frequency shift at 60 km. On the other hand, for the double pulse train induced by input (11), the peak power increases, and the FWHM decreases, with the increase of the modulation intensity, which implies that this input can be used to generate the pulse train with the higher peak power and narrower

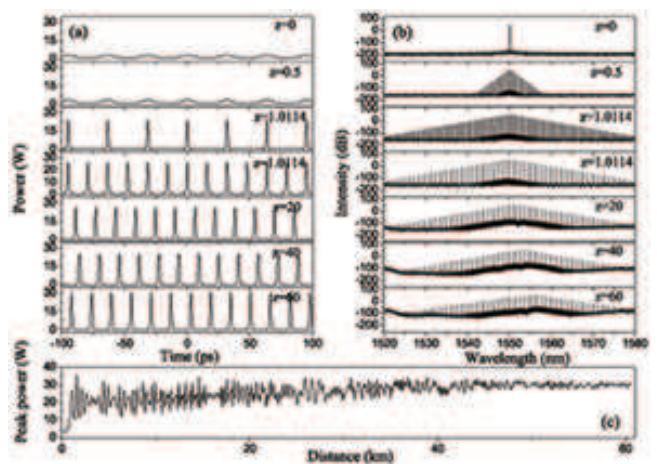


FIG. 6: (Color online) The same as in Fig. 4 except for $A = 0.55$.

width. However, in the same case, the frequency shift at 60 km increases with the increase of the modulation intensity in a staircase fashion, as shown in Fig. 5(d). Furthermore, from Figs. 5(b) and (c) one can find that the corresponding soliton numbers are in the range of $1.2592 < N < 1.3412$, each pulse in the double pulse trains eventually reshaping into the fundamental soliton, as seen in Figs. 3(c) and 4(c). Comparing with Figs. 1(d) and 2(d), one can see that Raman effect is helpful for the formation of solitons over a shorter propagation distance, as was shown in a different context in Ref. [39].

From Fig. 5(c) it can be seen that the pulse width in the trains is less than 2 ps (here the pulse width is taken equal to $\text{FWHM}/1.763$ [34]), and it may fall in the subpicosecond range for larger values of modulation intensity A . These widths are small enough to make it necessary using the extended model based on Eq. (1), rather than the simple NLS equation which does not include higher-order terms. To additionally illustrate this point, we have performed simulations of the propagation dynamics of the train initiated by input (11) with $A = 0.55$ in the subpicosecond range. In this case, the maximally compressed pulse train is attained at a shorter distance $z = 1.0114$ km in comparison with Fig. 4. Subsequently, the use of the delay-line interferometer produces the double pulse train with the FWHM of the central pulse 1.4083 ps (the corresponding pulse width is 799 fs) and peak power 26.3165 W. The corresponding robust evolution of the double pulse train is shown in Fig. 6(a). Comparing with the results shown in Fig. 4, we conclude that the spectrum range is wider, the frequency shift is larger, and the peak power is higher because the pulse width becomes narrower, as seen in Figs. 6(b) and (c).

Note that the above considerations disregarded fiber loss, assuming that it might be compensated by gain. Here, we display an example which explicitly takes the loss into account, and the results are shown in Fig. 7, in which the maximally compressed pulse train is attained at a somewhat longer distance, i.e., $z = 3.1306$ km (it

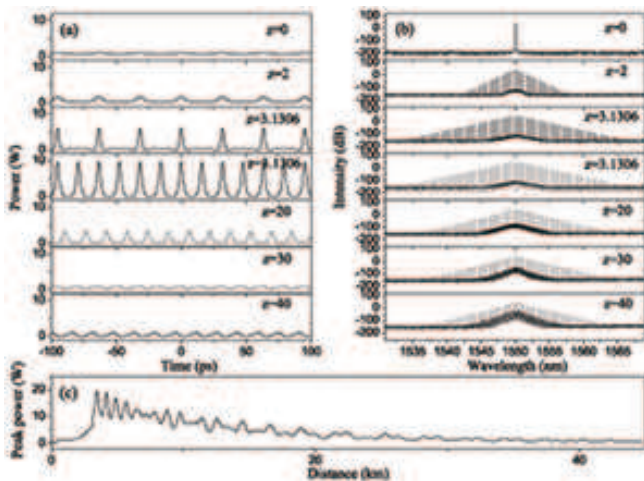


FIG. 7: (Color online) The same as in Fig. 4, but with fiber loss 0.19 dB/km.

was 2.9655km without fiber loss) and the peak power of the corresponding double pulse train is decreased to 9.6711 W, from 11.6262 W in the lossless fiber. Comparing with Fig. 4, we see that the propagation scenario is not strongly affected by the loss. Of course, the loss produces stronger effects over large propagation distances ($\gtrsim 30$ km), in which case periodic compensation provided by gain should be explicitly taken into account.

IV. CONCLUSIONS

Using exact solutions of the Hirota equation for the soliton on the finite background, including the AB

(Akhmediev breather) and KMS (Kuznetsov-Ma solution), the double high-power pulse trains with zero-background have been constructed. The results demonstrate that the double trains, built as superpositions of the maximally compressed pulse trains with opposite signs and a half-period time delay, propagate preserving their shape. The dynamics of the trains generated by the modulated CWs in the realistic fiber model has been simulated too, demonstrating that they can propagate robustly, with the red frequency shift caused by the Raman effect. Comparing different initial conditions, we have concluded that input (11) is more suitable for generating the pulse trains with a higher peak power and narrower width, the corresponding Raman-induced frequency shift being larger too, exhibiting a staircase dependence on the CW-modulation parameters. The settings analyzed in this work suggest an experimental realization in nonlinear optical fibers.

V. ACKNOWLEDGMENT

This research is supported by the National Natural Science Foundation of China grant 61078079 and 61475198, the Shanxi Scholarship Council of China grant 2011-010.

-
- [1] C. Kharif, E. Pelinovsky, and A. Slunyaev, *Rogue Waves in the Ocean*, (Springer, Heidelberg, 2009).
 - [2] C. Kharif and E. Pelinovsky, "Physical mechanisms of the rogue wave phenomenon," *Eur. J. Mech. B/Fluids* **22**, 603-634 (2003).
 - [3] A. Slunyaev, "Nonlinear analysis and simulations of measured freak wave time series," *Eur. J. Mech. B/Fluids* **25**, 621-635 (2006).
 - [4] V. E. Zakharov, A. I. Dyachenko, and A. O. Prokofiev, "Freak waves as nonlinear stage of Stokes wave modulation instability," *Eur. J. Mech. B/Fluids* **25**, 677-692 (2006).
 - [5] V. P. Ruban, "Nonlinear stage of the Benjamin-Feir instability: three-dimensional coherent structures and rogue waves," *Phys. Rev. Lett.* **99**, 044502 (2007).
 - [6] Andonowati, N. Karjanto, and E. van Groesen, "Extreme wave phenomena in down-stream running modulated waves," *App. Math. Mod* **31**, 1425-1443 (2007).
 - [7] D. R. Solli, C. Ropers, P. Koonath, and B. Jalali, "Optical rogue waves," *Nature (London)* **450**, 1054-1057(2007).
 - [8] N. Akhmediev, J. M. Soto-Crespo, and A. Ankiewicz, "Extreme waves that appear from nowhere: On the nature of rogue waves," *Phys. Lett. A* **373**, 2137-2145 (2009).
 - [9] B. Kibler, J. Fatome, C. Finot, G. Millot, F. Dias, G. Genty, N. Akhmediev, and J. M. Dudley, "The Peregrine soliton in nonlinear fibre optics," *Nature Physics* **6**, 790-795 (2010).
 - [10] B. Kibler, J. Fatome, C. Finot, G. Millot, G. Genty, B. Wetzal, N. Akhmediev, F. Dias, and J. M. Dudley, "Observation of Kuznetsov-Ma soliton dynamics in optical fibre," *Sci. Rep.* **2**, 463-467 (2012).
 - [11] K. Hammani, B. Kibler, C. Finot, Ph. Morin, J. Fatome, J. M. Dudley, and G. Millot, "Peregrine soliton generation and breakup in standard telecommunications fiber," *Opt. Lett.* **36**, 112-114 (2011).
 - [12] M. Erkintalo, K. Hammani, B. Kibler, C. Finot, N. Akhmediev, J. M. Dudley, and G. Genty, "Higher-order modulation instability in nonlinear fiber optics," *Phys. Rev. Lett.* **107**, 253901 (2011).
 - [13] H. N. Chan, K. W. Chow, D. J. Kedziora, R. H. J. Grimshaw, and E. Ding, "Rogue wave modes for a derivative nonlinear Schrodinger model," *Phys. Rev. E* **89**,

- 032914 (2014).
- [14] E. A. Kuznetsov, "Solitons in a parametrically unstable plasma," *Sov. Phys. Dokl.* **22**, 507-508 (1977).
- [15] Y. C. Ma, "The perturbed plane-wave solutions of the cubic Schrödinger equation," *Stud. Appl. Math.* **60**, 43-58 (1979).
- [16] N. Akhmediev and V. I. Korneev, "Modulation instability and periodic solutions of the nonlinear Schrödinger equation," *Theor. Math. Phys.* **69**, 1089-1093 (1986).
- [17] D. H. Peregrine, "Water waves, nonlinear Schrödinger equations and their solutions," *J. Austral. Math. Soc. Ser. B* **25**, 16-43 (1983).
- [18] J. M. Dudley, G. Genty, F. Dias, B. Kibler, and N. Akhmediev, "Modulation instability, Akhmediev breathers and continuous wave supercontinuum generation," *Opt. Express* **17**, 21497-21508 (2009).
- [19] B. Frisquet, B. Kibler, and G. Millot, "Collision of Akhmediev breathers in nonlinear fiber optics," *Phys. Rev. X* **3**, 041032 (2013).
- [20] A. Bendahmane, A. Mussot, P. Szriftgiser, O. Zerkak, G. Genty, J. M. Dudley, and A. Kudlinski, "Experimental dynamics of Akhmediev breathers in a dispersion varying optical fiber," *Opt. Lett.* **39**, 4490-4493 (2014).
- [21] B. Frisquet, A. Chabchoub, J. Fatome, C. Finot, B. Kibler, and G. Millot, "Two-stage linear-nonlinear shaping of an optical frequency comb as rogue nonlinear-Schrödinger-equation-solution generator," *Phys. Rev. A* **89**, 023821 (2014).
- [22] G. Y. Yang, L. Li, and S. T. Jia, "Peregrine rogue waves induced by the interaction between a continuous wave and a soliton," *Phys. Rev. E* **85**, 046608 (2012).
- [23] J. M. Dudley, G. Genty, and B. Eggleton, "Harnessing and control of optical rogue waves in supercontinuum generation," *Opt. Express* **16**, 3644-3651 (2008).
- [24] D. R. Solli, C. Ropers, and B. Jalali, "Active control of rogue waves for stimulated supercontinuum generation," *Phys. Rev. Lett.* **101**, 233902 (2008).
- [25] A. Mussot, A. Kudlinski, M. Kolobov, E. Louvergneaux, M. Douay and M. Taki, "Observation of extreme temporal events in CW-pumped supercontinuum," *Opt. Express* **17**, 17010-17015 (2009).
- [26] M. Taki, A. Mussot, A. Kudlinski, E. Louvergneaux, M. Kolobov, and M. Douay, "Third-order dispersion for generating optical rogue solitons," *Phys. Lett. A* **374**, 691-695 (2010).
- [27] J. Fatome, B. Kibler, and C. Finot, "High-quality optical pulse train generator based on solitons on finite background," *Opt. Lett.* **38**, 1663-1665 (2013).
- [28] C. Mahnke, and F. Mitschke, "Possibility of an Akhmediev breather decaying into solitons," *Phys. Rev. A* **85**, 033808 (2012).
- [29] C. Mahnke, and F. Mitschke, "Ultrashort light pulses generated from modulation instability: background removal and soliton content," *Applied Phys. B* **116**, 15-20 (2013).
- [30] G. Y. Yang, L. Li, S. T. Jia, and D. Mihalache, "High power pulses extracted from the Peregrine rogue wave," *Rom. Rep. Phys.* **65**, 391-400 (2013).
- [31] G. Y. Yang, L. Li, S. T. Jia, and D. Mihalache, "Controlling high power pulses extracted from maximally compressed pulse in a nonlinear optical fiber," *Rom. Rep. Phys.* **65**, 902-914 (2013).
- [32] G. Y. Yang, Y. Wang, Z. Qin, B. A. Malomed, D. Mihalache, and L. Li, "Breatherlike solitons extracted from the Peregrine rogue wave," *Phys. Rev. E* **90**, 062909 (2014).
- [33] Y. Kodama and A. Hasegawa, "Nonlinear pulse propagation in a monomode dielectric guide," *IEEE J. Quantum Electron.* **23**, 510-524 (1987).
- [34] G. P. Agrawal, *Nonlinear Fiber Optics* (Academic Press, New York, 1995).
- [35] R. Hirota, "Exact envelope-soliton solutions of a nonlinear wave equation," *J. Math. Phys.* **14**, 805-809 (1973).
- [36] S. Li, Lu Li, Z. Li, and G. Zhou, "Properties of soliton solutions on a cw background in optical fibers with higher-order effects," *J. Opt. Soc. Am. B* **21**, 2089-2094 (2004).
- [37] A. Ankiewicz, J. M. Soto-Crespo, and N. Akhmediev, "Rogue waves and rational solutions of the Hirota equation," *Phys. Rev. E* **81**, 046602 (2010).
- [38] M. Erkintalo, G. Genty, B. Wetzal, and J. M. Dudley, "Akhmediev breather evolution in optical fiber for realistic initial conditions," *Phys. Lett. A* **375**, 2029-2034 (2011).
- [39] P. V. Mamyshv, S. V. Chernikov, E. M. Dianov, and A. M. Prokhorov, "Generation of a high-repetition-rate train of practically noninteracting solitons by using the induced modulational instability and Raman self-scattering effects," *Opt. Lett.* **15**, 1365-1367 (1990).